Hindawi
Mathematical Problems in Engineering
Volume 2019, Article ID 9518437, 12 pages
https://doi.org/10.1155/2019/9518437

Research Article

Ricochet Characteristics of AUVs during Small-Angle Water Entry Process

Guo-Xin Yan,[1,2] Guang Pan ,[1,2] and Yao Shi[1,2]

[1]*School of Marine Science and Technology, Northwestern Polytechnical University, Xi'an 710072, China*
[2]*Key Laboratory of Unmanned Underwater Vehicle, Northwestern Polytechnical University, Xi'an 710072, China*

Correspondence should be addressed to Guang Pan; panguang@nwpu.edu.cn

Received 9 August 2019; Accepted 11 December 2019; Published 28 December 2019

Academic Editor: Hao Zhang

When the autonomous underwater vehicle (AUV) enters the water at a small angle, the head of the AUV will be subjected to a torque that causes it to rise, which may cause the AUV to ricochet. The occurrence of ricochet will have an important impact on the trajectory stability of the AUV. In this paper, the finite element method-smoothed particle hydrodynamics (FEM-SPH) coupling algorithm, which absorbs the high efficiency of FEM and the advantages of SPH in dealing with large deformation and meshes distortion, is used to study the small-angle water entry problem of the AUV numerically. In the coupled FEM-SPH algorithm, discrete particles were used to model the zone of water, while the part of the AUV was modeled with finite elements. A contact algorithm couples the finite elements and the particles. Particular attention was paid to the influence of different head hemisphere angles and different initial conditions on the ricochet trajectory of the AUV. The critical conditions and influencing factors of the AUV ricochet phenomenon were given.

1. Introduction

Current autonomous underwater vehicles (AUVs) are particularly useful as unmanned measurement platforms that carry sensor payloads along preprogrammed trajectories to collect data for various applications such as hydrographic survey, undersea oil/gas production, hull inspection, military applications, and so on [1]. When the vehicle launches, it will inevitably encounter the problem of water entry, especially the air-launched autonomous underwater vehicles (AUVs).

The problem of water entry has been applied in many applications. Basilisk lizard walking on water can also be regarded as an interesting phenomenon of entering water [2], the military application such as the initial impact of air-launched marine vehicle [3] or torpedo [4], and aerospace engineering such as aircraft forced landing on water [5].

The research on water entry problems mainly focuses on the following three aspects: the evolution process of water entry cavitation, calculating the water impact forces, especially during the initial entry stages, where the maximum impact loads occur, and the analysis of water entry trajectory. One of the fascinating problems in hydrodynamics is the ricocheting of a rigid body off a free water surface. A ricochet may occur when the body hits the free surface at grazing angles with relatively high impact speed. Ricochet studies are essential for both offensive and defensive modes of action. In offensive applications, a typical example is "bouncing bomb," a weapon designed by Sir Barnes Wallis for attacking dams during the Second World War. On the other hand, in defensive applications, it helps in determining the initial launch conditions of the projectile to avoid ricochet, which may cause damage to the projectile structure or lead to missing its intended target [6]. Furthermore, the mathematics involved in ricochet also helps seaplanes to land accurately and improve the design of the airplane wing.

The research of Richardson [7] dealt somewhat with ricochet and presented experimental results concerning the water entry of ebonite and duralumin spheres at different angles of impact. Besides, the records of splash performance

and force-penetration curves were given. Since the hydrodynamical aspects of the ricochet phenomenon are rather complicated, it is quite challenging to solve the problem theoretically. Nevertheless, early investigations of the phenomenon, reviewed by Johnson and Reid [8], showed the following surprisingly simple empirical formula for the critical angle of incidence, θ_c:

$$\theta_c = \frac{18^\circ}{\sqrt{\sigma}}, \tag{1}$$

where σ is the specific gravity of the projectile. Thus, if the water entry angle of a spherical projectile is larger than θ_c, a ricochet of a projectile from the water will not occur, and the heavy projectile will sink into the water. Miloh and Shukron [9] obtained the actual trajectory of the sphere below the free surface by the integration of Kelvin–Kirchoff–Lagrange equations, and critical value for the projectile ricochet was obtained in terms of the initial Froude number and the specific density of the solid. It is demonstrated that for infinitely large Froude numbers, the solution was in surprisingly good agreement with the empirical relationship (equation (1)) for the critical angle of a sphere in oblique water entry.

The aforementioned works have not considered the effect of the rotation of the sphere on the ricochet. Truscott and Techet [10] investigated the complex hydrodynamics of water entry of a spinning sphere for low Froude numbers experimentally. High-speed digital video sequences revealed the unique hydrodynamics phenomena, which vary with spin rate and impact velocity. They found that the spinning motion induces a lift force on the sphere and thus causes noticeable curvature in the trajectory of the sphere along its descent. In the study of disc-shaped stone skipping by Bocquet et al. [11–13], they believed that the angular motion of stone gyroscopically maintains the attack angle. Moreover, they revealed that there exists a "magic angle" of 20° between a disk face and free water surface which minimizes the required speed for ricochet.

The elastic deformation of the sphere is another important aspect of studying its ricochet characteristics. Truscott et al. [14]and Belden et al. [15] investigated the skipping of highly compliant elastomeric spheres to interpret the mechanisms by which they ricochet off the water. They demonstrated that, unlike stone skipping, the elasticity of the sphere plays an important role in determining the success of the ricochet through experimental and numerical study.

Although many scholars have carried out research on the problem of water entry ricochet and obtained some rules of the cavity, impact load, and trajectory during the water entry process, the research objects are mostly projectiles, small spheres, or stones. The research on the mechanism of small-angle water entry ricochet of some slightly complicated vehicle is quite rare. To our knowledge, Park et al. [16] studied numerically the impact and ricochet problems of arbitrary-shaped water entry bodies using the source panel method. Unfortunately, they did not give a more detailed and systematic analysis of the ricochet trajectory. Wang and Shi [17] carried out a numerical simulation using the arbitrary Lagrange–Euler (ALE) coupling method to study dynamic mechanical properties of the oblique water entry hydroballistics of an air-borne missile. Moreover, they believed that the initial curvature of the ogive with a smaller mass is larger, which makes it easy to produce ricochet behavior.

Finite element method (FEM) as a conventional grid-based numerical method has been widely applied to various areas of computational fluid dynamics (CFD) and currently is the dominant method in numerical simulations of domain discretization and numerical discretization. However, for the problem with extreme distortions, the accuracy of FEM is not always adequate [18].

In the aspect of coupled numerical algorithm of water entry problem, Paik et al. [19], Maki et al. [20], and Xie et al. [21] have adopted the coupled CFD-FEM method to simulate the hydroelastic impact of a composite structure. However, this method is usually used to analyze the structural response of the elastomer and obtain the maximum shape variables of the structure. The simulation accuracy of the evolution of the convection field with time is slightly poor. The DEM-SPH method is suitable for dealing with the coupling problem between granular materials and fluid dynamics, but as a pure meshless method, it usually consumes a lot of computing resources. In this way, the coupled FEM-SPH algorithm seems to be a reasonable approach which absorbs both the high efficiency of FEM and the advantages of SPH algorithm in dealing with large deformation and meshes distortion.

Despite some literature studies [22–25] involving the influence of the head shape of the model on the water entry impact, there are few specific investigations that focus on the impact of the head shape on the trajectory characteristics during the process of water entry. The lift and pitching moments are important components of the hydrodynamic force system which affect the trajectory of the vehicle significantly when the vehicle impacts the water surface obliquely at high speed. Therefore, the aim of this paper is to adopt the coupled FEM-SPH method to study the ricochet characteristics of the high-speed water entry of vehicle numerically and obtain the effects of head shapes and initial entry conditions on the ricochet characteristics. This will provide a reference for the safe high-speed water entry and trajectory control strategies of the AUV.

2. Numerical Method and Model

2.1. SPH Methodology. The process of high-speed water entry of a marine vehicle is quite complicated, which involves the problem of unsteady motion and interactions of air, water, and vehicle body. The solution of the ricochet problem is greatly dependent on the change in the highly nonlinear boundary morphology of the free water surface, which makes the problem difficult to solve analytically. The fundamental idea of the meshfree methods is to provide accurate and stable numerical solutions for integral equations or partial differential equations (PDEs) with all kinds of possible boundary conditions with a set of arbitrarily

distributed particles (or nodes) without using any mesh that provides the connectivity of these particles or nodes. The smoothed particle hydrodynamics (SPH) method is a meshfree particle method of adaptive and pure Lagrangian nature and is attractive in treating large deformation, tracking moving interfaces or free surfaces, and obtaining the time history of the field variables [26]. Since its invention to solve astrophysical problems in three-dimensional open space [27, 28], SPH has been extensively studied and extended to dynamic fluid flows with large deformations, including the water entry problems [29–32].

The core idea of the SPH approach is as follows: (1) the problem domain is represented by a set of arbitrarily distributed particles; (2) the integral representation method is used for field function approximation; (3) the kernel approximation is then further approximated using particles; (4) the particle approximations are performed to all terms related to field functions in the PDEs to produce a set of ODEs in discretized form with respect to time only; and (5) the ODEs are solved using an explicit integration algorithm to achieve fast time stepping and to obtain the time history of all the field variables for all the particles.

In the SPH method, the state of a system is represented by a set of particles, which possess individual material properties and move according to the governing conservation equations. For a given particle i which carries its own velocity, density, mass, and pressure, by applying the particle approximation, a function f can be expressed by the following:

$$\langle f(x_i)\rangle = \sum_{j=1}^{N} \frac{m_j}{\rho_j} f\left(x_j\right) W_{ij}, \tag{2}$$

where $W_{ij} = W(|x_i - x_j|, h)$ is the smoothing kernel function and is closely related to the smoothing length h, N is the number of particles in the support domain of particle i, and m_j and ρ_j are the mass and density associated with particle j, respectively. The most commonly used smoothing kernel function is a cubic B-spline:

$$W\left(\left|x_i - x_j\right|, h\right) = C \times \begin{cases} 1 - \frac{3}{2}d^2 + \frac{3}{4}d^3, & 0 \le d < 1, \\ \frac{1}{4}(2-d)^3, & 1 \le d < 2, \\ 0, & \text{otherwise}, \end{cases} \tag{3}$$

where C is a constant of normalization that depends on the space dimension and d is defined as

$$d = \frac{\left|x_i - x_j\right|}{h_{\text{avg}}}, \tag{4}$$

where h_{avg} is the average value of smoothing length of the two particles being considered.

The equations of conservation laws of continuum fluid dynamics, including conservation of mass, conservation of momentum, and conservation of energy, can be expressed as follows:

$$\begin{aligned} \frac{\mathrm{d}\rho_i}{\mathrm{d}t} &= \sum_{j=1}^{N} m_j v_{ij}^{\beta} = \left(v_i^{\beta} - v_j^{\beta}\right) \cdot \frac{\partial W_{ij}}{\partial x_i^{\beta}}, \\ \frac{\mathrm{d}v_i^{\alpha}}{\mathrm{d}t} &= \sum_{j=1}^{N} m_j \left(\frac{\sigma_i^{\alpha\beta}}{\rho_i^2} + \frac{\sigma_j^{\alpha\beta}}{\rho_j^2}\right) \cdot \frac{\partial W_{ij}}{\partial x_i^{\alpha}}, \\ \frac{\mathrm{d}E_i}{\mathrm{d}t} &= \frac{1}{2} \sum_{j=1}^{N} m_j \left(\frac{p_i}{\rho_i^2} + \frac{p_j}{\rho_j^2}\right) v_{ij}^{\beta} \frac{\partial W_{ij}}{x_i^{\beta}}, \end{aligned} \tag{5}$$

where α and β are used to denote the coordinate directions and σ is the total stress tensor.

Moreover, the Monaghan [33] type linear artificial viscosity Π_2 is added for removing numerical oscillations in hydrodynamics. The detailed formulation is as follows:

$$\begin{aligned} p_i &\longrightarrow p_i + \Pi_{ij}, \\ \Pi_{ij} &= \begin{cases} \dfrac{-\alpha \overline{c}_{ij} \mu_{ij} + \beta \mu_{ij}^2}{\overline{\rho}_{ij}}, & v_{ij} \cdot x_{ij} < 0, \\ 0, & \text{otherwise}, \end{cases} \\ \mu_{ij} &= \frac{\overline{h}_{ij} v_{ij} \cdot x_{ij}}{\left|x_{ij}\right|^2 + \varphi^2}, \end{aligned} \tag{6}$$

where α and β are constants that are all typically set around 1.0 and c and $\mathbf{v}$ represent the speed of sound and the particle velocity vector, respectively. The notation $\overline{X}_{ij} = (1/2)(X_i + X_j)^{-}$ is used for median between X_i and X_j. Here, $\mathbf{v}_{ij} = (\mathbf{v}_i - \mathbf{v}_j)$ and $\mathbf{x}_{ij} = (\mathbf{x}_i - \mathbf{x}_j)$, and φ prevents the denominator from vanishing.

2.2. Design of the Vehicle Model. In order to explore the impact of vehicle geometry on the ricochet behavior, we have designed five different head shapes of model with reference to the Waugh's [34] study. The head shapes and parameters' definition are shown in Figure 1. The spherical portion is expressed in terms of the half-sphere angle, i.e., the angle subtended by the generating curve of the spherical head measured from the tip of the head to the point of junction with the ogival curve.

The eight models of vehicle with different head shapes are shown in Figure 2, and the specific parameters of the vehicle are shown in Table 1.

2.3. The Coupled FEM-SPH Model. In the study of the ricochet of the high-speed vehicle, the deformation of the vehicle is extremely small, so we assume it as a rigid body. But, the water will cause great deformation due to the splash. Therefore, we use the FEM-SPH coupling algorithm for numerical simulation. Since both SPH and FEM are based on the Lagrangian description, it is easy to handle the interaction of the fluid-solid interface through the penalty-type "nodes-to-surface" contact algorithm where finite elements of the vehicle are treated as the master segments and

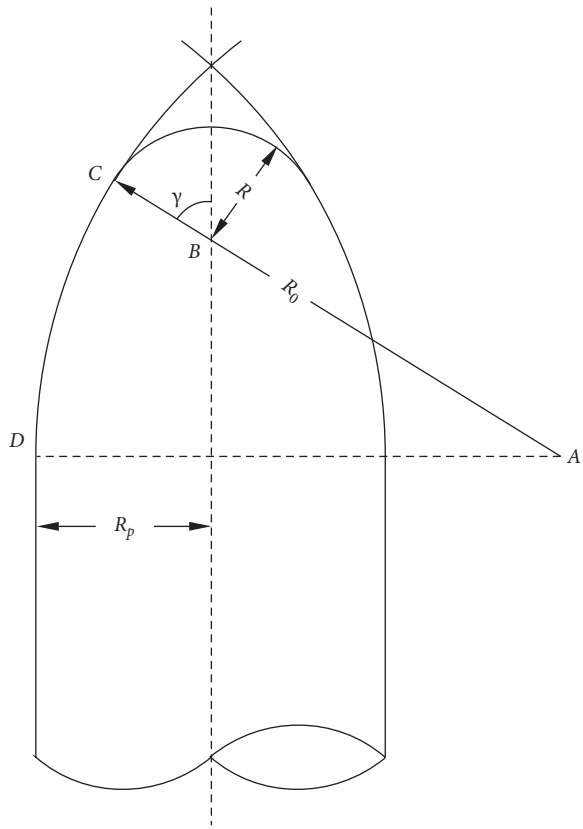

A Center of curvature of ogive
B Center of curvature of sphere
C Junction of sphere and ogive
D Junction of ogive and cylinder
R Sphere radius
R_0 Ogival radius
R_P Body or projectile radius
γ Half-sphere angle

Figure 1: Head shapes and parameters' definition of the vehicle.

SPH particles of water are treated as the slave nodes as shown in Figure 3. The calculation of the contact algorithm comprises two stages: contact search and contact force calculation. The contact partners are detected when a slave node penetrates the contact area of a master element. Then, the contact force is calculated by penetration depth and contact stiffness. Consequently, the particle experiences a repelling contact force in the direction of the surface normal and the finite elements belonging to the master segment in contact proportionately bear this force in opposite direction. The specific coupling process is shown in Figure 4.

The vehicle body is divided into Lagrangian grids, and the water domain is discretized by smooth particles. Moreover, the boundary conditions of water domain at symmetry planes were imposed using a specific boundary condition treatment according to which a set of ghost particles is automatically created by reflecting the particles closest to the boundaries.

According to Chuang's point of view [35], we choose the calculation domain size as $6 \times 2 \times 2$ m. In this paper, the space between the Lagrange grids is 25 mm, and the SPH particles are evenly distributed with an interval of 40 mm. The total number of particles and solid elements used during our simulations is 375000 and 11424, respectively. We set the simulation termination time to 50 ms, where each case takes about 2.5 hours. It should be noted that our computer's processor is a quadcore 8-thread Intel Core i7 4790 clocked at 3.6 GHz with 16G memory.

The description of the FEM-SPH model and coordinate definition are shown in Figure 5. The coordinate origin O is the center of gravity of the vehicle. The coordinate systems $Oxyz$ and $Ox_1y_1z_1$ are the body coordinate system and the velocity coordinate system of the vehicle, respectively. The line OP in Figure 5(b) is the projection of the velocity axis Ox_1 on the plane of the body coordinate system $Oxyz$. The angle between the Ox axis and the horizontal plane is defined as the water entry angle θ; the angle between OP and vehicle longitudinal axis Ox is called the attack angle α which is positive when OP is below the Ox axis from the rear of the vehicle.

3. Numerical Results and Discussion

The process of small-angle water entry of AUV can be roughly divided into three stages: the stage of head impacting the water, the stage of tail rudder hitting the water, and the stage of ballistic stabilization. We take the water entry process of a AUV with a half-sphere angle of 60° as an example. When the initial velocity of water entry is 100 m/s and the initial angle of water entry is 20°, we can see from Figure 6 that during the period of 0 ~ 10 ms, the head of the AUV gradually impacts the water and produces a water surface uplift. Then, immediately at about 20 ms, the rudder of the AUV began to hit the water, causing a strong splash of water near the rear. During the period of 40 ~ 50 ms, the trajectory of the AUV gradually stabilized. In this process, the reaction force on the head and tail rudder will lead to a great change in the trajectory of the vehicle; that is to say, the head of the vehicle will have a tendency to rise first and then sink.

Correspondingly, as can be seen from Figure 7, when the aircraft with a hemispherical angle of 0° enters the water at an initial water impact angle of 15° and a velocity of 100 m/s, the head of the vehicle collides with the water surface, and then the head of the vehicle jumps out of the water under the action of the lifting moment, resulting in ricocheting phenomenon. Next, we discuss in detail the effect of head shape of the AUV on this process.

3.1. Critical Conditions for Ricocheting. Given different initial water entry conditions, the influence of water entry angle, velocity, and angle of attack on ricochet phenomena was investigated.

Figure 8(a) shows that when the vehicle enters the water at no angle of attack, the occurrence of ricochet is restricted by both the angle of entry and the velocity. With the increase of water entry angle, the maximum speed of bouncing decreases gradually, and the minimum speed of bouncing

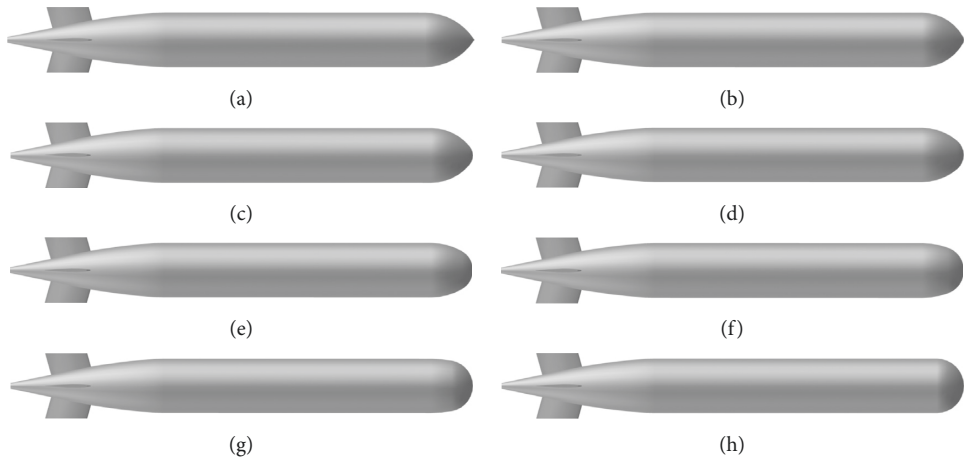

Figure 2: Eight vehicle models with different head shapes. (a) $\gamma = 0^{\circ}$. (b) $\gamma = 30^{\circ}$. (c) $\gamma = 40^{\circ}$. (d) $\gamma = 50^{\circ}$. (e) $\gamma = 60^{\circ}$. (f) $\gamma = 70^{\circ}$. (g) $\gamma = 80^{\circ}$. (h) $\gamma = 90^{\circ}$.

Table 1: Vehicle structural parameters.

Length (mm)	Diameter (mm)	Shell thickness (mm)	Mass (kg)	Material
1722	200	6.18	16	6061 aluminium alloy

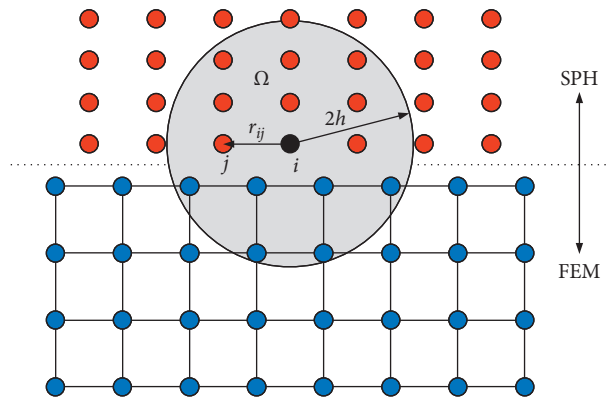

Figure 3: A contact force is applied between the particle i and all the FE nodes within $2h$. Ω represents the support domain of particle i.

increases gradually. Figure 9(a) shows that with the increase of angle of attack, the range of velocity to maintain the ricochet decreases gradually. A similar rule can be seen in Figure 9(b), that is, the range of the water entry angle to maintain the ricochet of the vehicle decreases with the increase of the angle of attack. However, when the angle of entry is 15°, it shows a special law, that is, when the angle of attack is about 5° to 15°, the vehicle will not ricochet. This is because in this angle of attack range, the pressure on the lower side of the head when the vehicle slams against the water surface counteracts the pressure on the downward side of the head when it slams against the water surface, thus maintaining its trajectory stability. In addition, we find that when the vehicle enters the water at 15°, the water outlet angle increases with the decrease of the absolute value of the angle of attack in the case of negative angle of attack and increases with the increase of the angle of attack in the case of positive angle of attack in the case of bouncing.

3.2. The Effect of Head Shape on Trajectory. The trajectory of the center point of the AUV model's head is selected to analyze the trajectory characteristics of the vehicle entering the water. Moreover, our analysis of trajectory characteristics is only for the initial stage of the water entry process, the prediction and control of the impact load and trajectory of the AUV in this stage are more complex, and it is even more necessary in the issue of safe water entry of the AUV. We have carried out a series of water entry simulations for different head shapes of AUVs at different water entry angles. It should be noted that in these simulations, we give the same impact velocity $v = 100$ m/s and the water impact time $t = 0.05$ s.

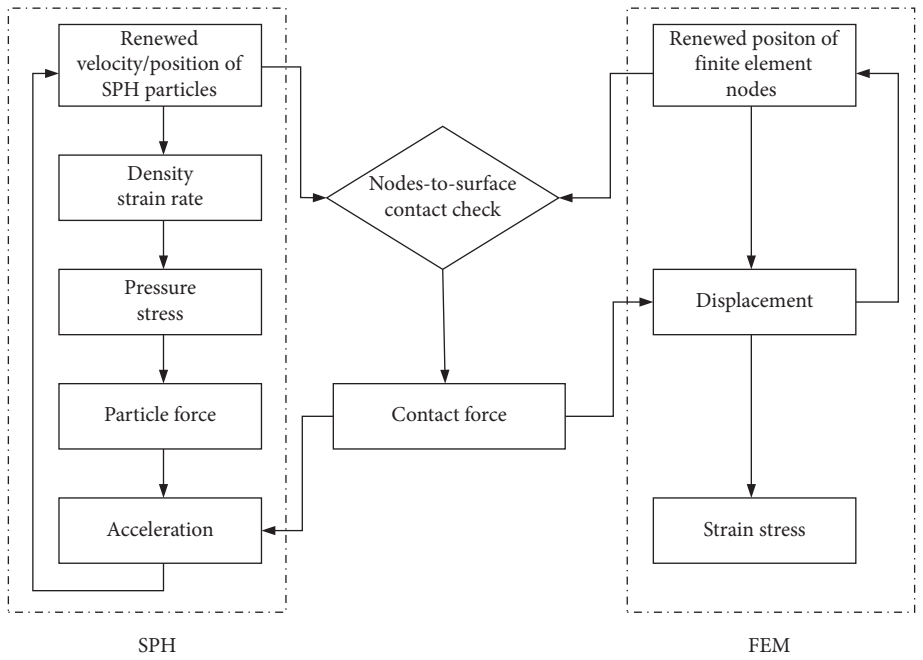

Figure 4: FEM-SPH coupling flowchart.

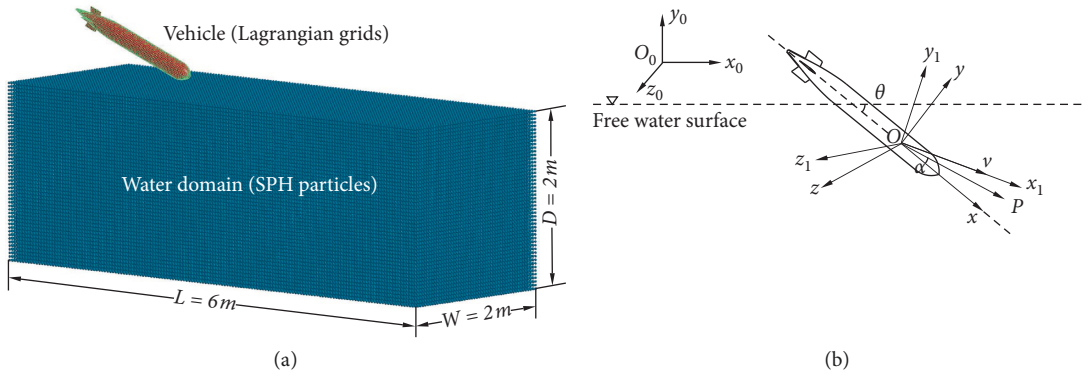

Figure 5: Description of the FEM-SPH model (a) and coordinate definition (b).

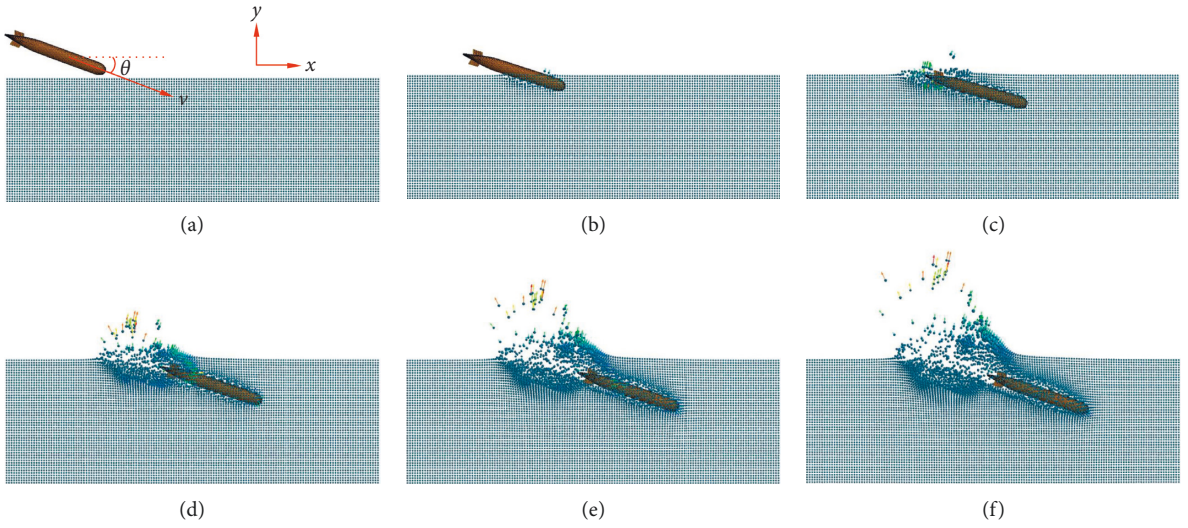

Figure 6: Water entry process of the AUV with $\gamma = 60^\circ$. The initial velocity of water entry is 100 m/s, and the initial angle of water entry is 20°. (a) $t = 0$ ms. (b) $t = 10$ ms. (c) $t = 20$ ms. (d) $t = 30$ ms. (e) $t = 40$ ms. (f) $t = 50$ ms.

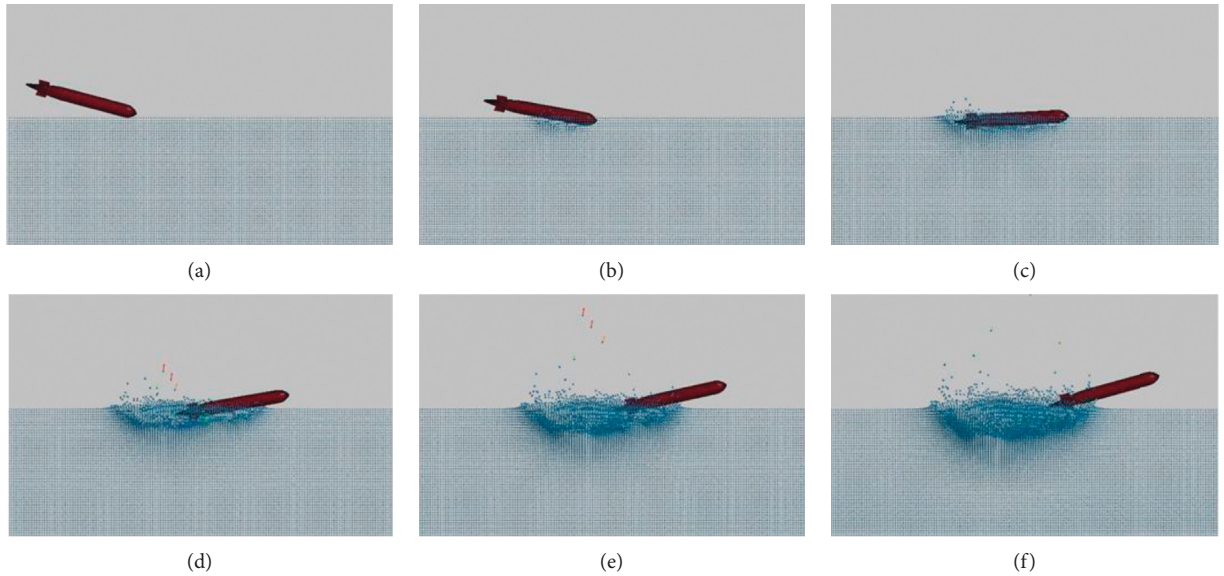

Figure 7: The ricocheting process of the AUV with $\gamma = 0^\circ$. The initial velocity of water entry is 100 m/s, and the initial angle of water entry is 15°. (a) $t = 0$ ms. (b) $t = 10$ ms. (c) $t = 20$ ms. (d) $t = 30$ ms. (e) $t = 40$ ms. (f) $t = 50$ ms.

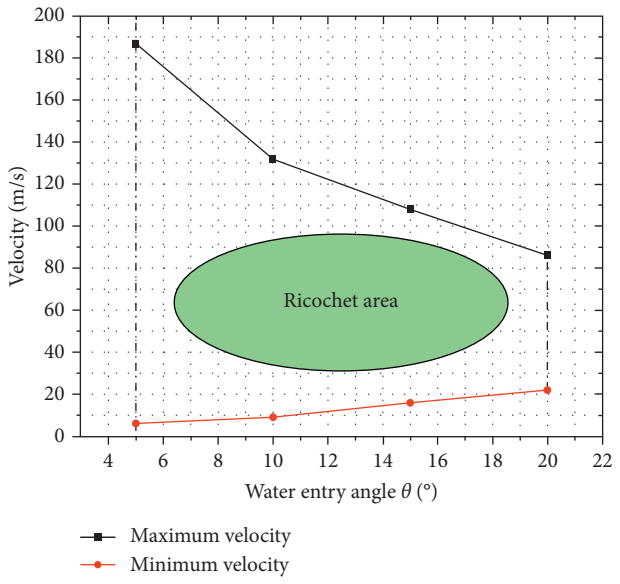

Figure 8: Ricochet area determined by critical angles and velocities of water entry.

From Figure 10(a), we can see that when the angle of water entry is 15°, the trajectory of the AUVs with different head shapes will be significantly different, and there may even be completely different changing trends. For example, when the half-sphere angle of the model head is 50°, the model has the tendency to ricochet off the water surface. The trajectories of other models do not have this evolution rule, but a relatively stable water entry. This shows that the water entry trajectory of the model is sensitive to the entry angle of 15°, and relatively large fluctuations will occur, which will affect the safe entry of the AUV. The reason for this result may be that when the model impacts the water surface at a 15° angle, the model with a 50° half-sphere angle has a larger water contact area and a

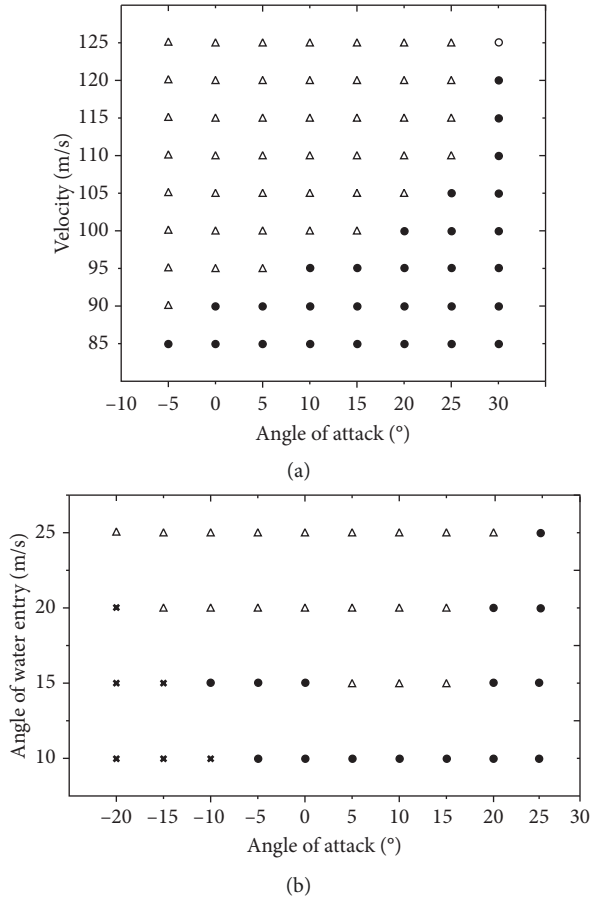

Figure 9: Statistical graphs of whether ricocheting phenomena occur under different water entry conditions. Δ, ·, and × represent no ricochet, ricochet, and no water entry, respectively. (a) The statistics of angle of attack, velocity, and ricochet when the water entry angle is 20 degrees. (b) The statistics of angle of attack, angle of water entry, and ricochet when the water entry velocity is 100 m/s.

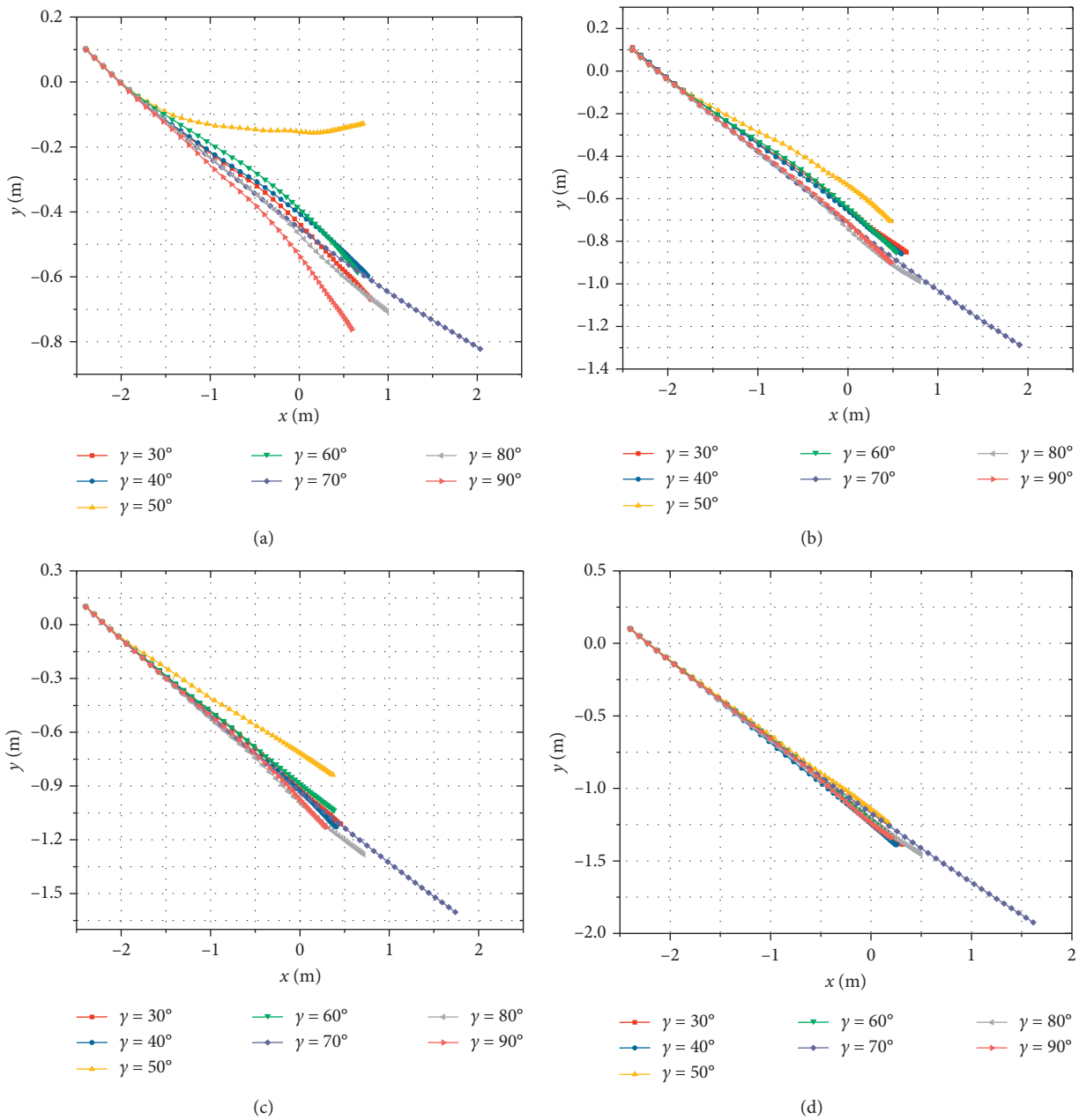

Figure 10: Trajectory curves of the AUVs with different head shapes at variable water entry angles. The velocity of water entry is fixed at 100 m/s. (a) $\theta = 15^{\circ}$. (b) $\theta = 20^{\circ}$. (c) $\theta = 25^{\circ}$. (d) $\theta = 30^{\circ}$.

stronger water reaction force in the initial stage, resulting in the head of the model to have a larger lifting torque.

On the other hand, a special phenomenon can be seen from Figure 10, that is, when the half-sphere angle of the model's head is 70°, the lateral distance of the model moving underwater at the same time is the longest and the depth of the water entry is also deepest. The cause of this phenomenon is also related to the stress environment of head of the model. The model with a half-sphere angle of 70° has the smallest navigational resistance during the initial stage of water entry.

On the whole, the influence of the head shape of the AUV on the trajectory characteristics gradually decreases with the increase of the water entry angle, and the entry trajectories of AUVs become more and more stable.

In addition to the angle of water entry, the influence of the head shape of the AUV on the trajectory at different entry velocity is also different. Figure 11 shows the trajectory curves of the AUVs with different head shapes at variable water entry velocities. The angle of water entry is fixed at 15°; however, the simulation time of the water impact of the AUVs is 0.08 s, 0.05 s, 0.03 s, and 0.025 s, respectively, when the impact velocity is 50 m/s, 100 m/s, 150 m/s, and 200 m/s. The cross section at the ordinate $y = 0$ m represents the horizontal plane. If the longitudinal coordinates of the

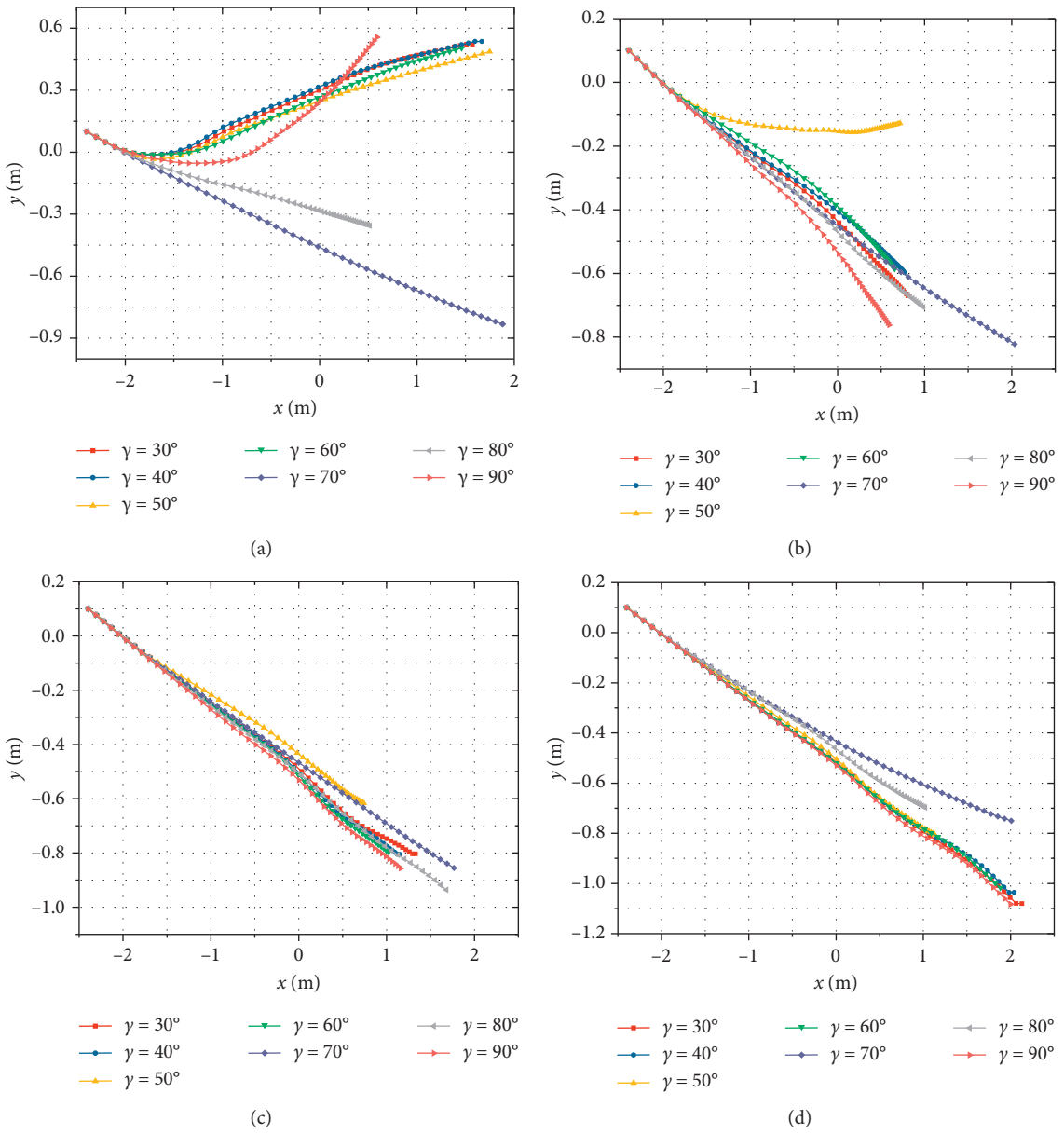

Figure 11: Trajectory curves of the AUVs with different head shapes at variable water entry velocities. The angle of water entry is fixed at 15°. (a) $v = 50$ m/s. (b) $v = 100$ m/s. (c) $v = 150$ m/s. (d) $v = 200$ m/s.

center point of the head of an AUV is greater than 0, then we say that the AUV has ricocheted.

As can be seen from Figure 11(a), when the velocity of water entry is 50 m/s, the bouncing phenomenon occurs in all the vehicles except for the cases of $\gamma = 70°$ and $\gamma = 80°$. It is worth noting that in this figure, the trajectory curve of the AUV with a hemispheric angle of 90° changes drastically, resulting in the highest ricochet height. The reason for this phenomenon is that the diameters of the open cavities are different when the AUVs with different hemispheric angles impact the water surface at the same velocity. The larger the hemispheric angle of the head, the larger the diameter of the open cavity. When $\gamma = 90°$, the diameter of the open cavity of the model head is sufficiently large that the recovery torque generated when the rudder touches the water becomes small. The imbalance of the head and tail torques of the model results in ricocheting.

In terms of the overall trajectory curves, when the angle of water entry is constant ($\theta = 15°$), the stability of the water entry trajectory has a tendency to increase first and then decrease as the velocity of water entry increases. Moreover, combined with the full figure, it can be also seen that the vehicle with a hemispherical angle of 70° or 80° has better trajectory stability of water entry, which is of great significance to the attitude control of the AUV.

3.3. The Effect of Impact Velocity on Trajectory. As can be seen from Figure 12, keeping the other inflow conditions unchanged, when the inflow velocity increases gradually, the

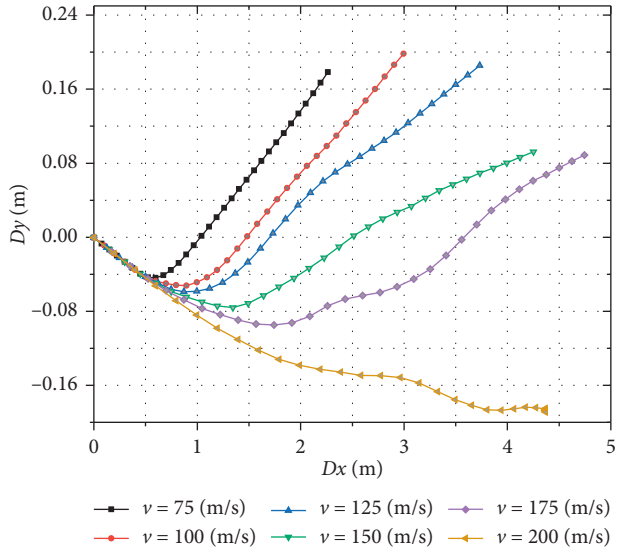

Figure 12: Trajectory curves of the AUVs with different head shapes at variable water entry velocities. The angle of water entry is fixed at 15°.

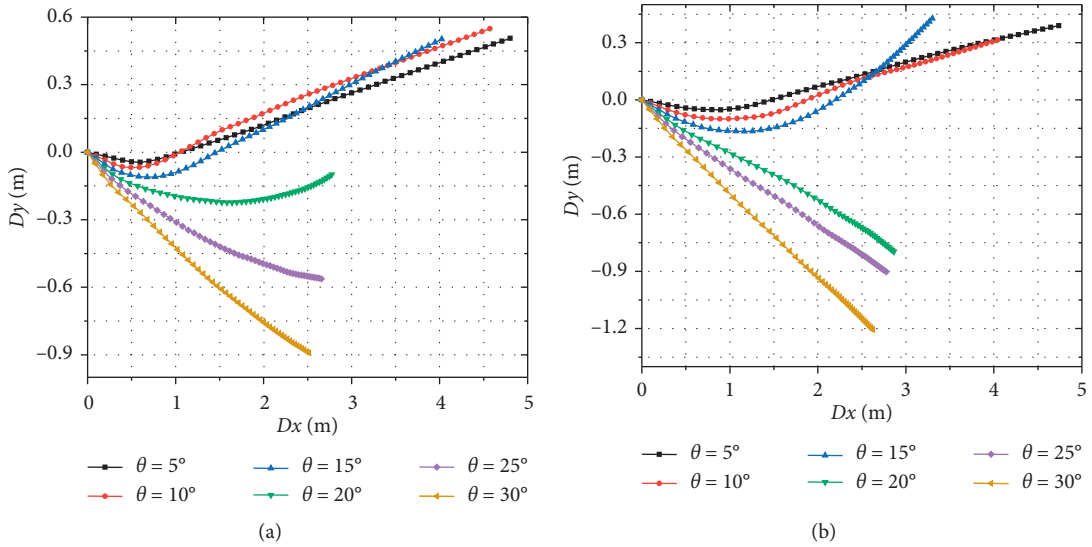

Figure 13: Trajectory curves of the AUVs at different water entry angles. Water entry velocities of (a) 50 m/s and (b) 100 m/s.

kinetic energy obtained by the model increases gradually, which leads to the increase of the navigation distance in the same time. However, after ricocheting, the water exit angle decreases gradually, and even when the water entry speed is 200 m/s, there is no ricochet phenomenon. We believe that the reason for this phenomenon is that when the velocity of the model increases gradually, the diameter of the open cavity caused by water impact increases gradually and the wetting area of the model's head changes so that the clockwise moments generated by the upstream and tail counterbalance the upward moments generated by the backflow surface. That is to say, the direction of the external forces on the model is closer to the center of gravity of the model, and the stability of the model trajectory is also higher and higher. For the same reason, the head exit angle (in the case of ricocheting) of the vehicle decreases gradually with the increase of the impact velocity.

3.4. The Effect of Angle of Water Entry on Trajectory. As can be seen from Figure 13, keeping the other initial water entry conditions unchanged, the vertical displacement of the model increases with the increase of the water entry angle, which means that the rising trend of the initial inflow model becomes more and more insignificant. In the case of ricocheting, the water exit angle of the vehicle decreases gradually. The reason for this phenomenon is that the change of the initial water entry angle will directly affect the diameter of the opening cavity and the wetted area of the model during the water entry process, which are two important factors affecting the force of the model head. The same rule applies to situations where no ricochet occurs.

Comparing Figures 13(a) and 13(b), it can be seen that the impact of water entry velocity on ricochet cannot be ignored. When the water entry angle of the model is 15° and 20°, the ricochet phenomenon is more sensitive to the

change of water entry velocity. In addition, we can see that the occurrence of ricochet phenomenon makes the horizontal displacement of the vehicle increase greatly at the same time, which is an important concern of the trans-medium vehicle.

4. Conclusions

In the initial stage of water entry, the fluid medium will be vigorously moved by the AUV. At the same time, the sudden changes in the trajectory, strain, and acceleration caused by the impact will cause damage to the structure of the AUV and failure of the electronic components. Especially when the AUV enters the water at a small angle, it may cause ricochet phenomenon, which poses a greater threat to the safe water entry of the vehicle. Therefore, it is of great significance to carry out research on the trajectory characteristics in the initial stage of water entry.

In this paper, the coupled FEM-SPH algorithm which combined the efficiency of FEM and the advantages of SPH in dealing with the large deformation problems is used to numerically study the small-angle water entry problems of the AUV. Specifically, a penalty contact algorithm is used to couple the discrete finite elements of the AUV with the discrete particles of the water, and ghost particles are set around and the bottom of the water to simulate the infinite water area.

A series of simulation studies have been carried out under different initial water entry conditions, and the critical conditions for bouncing have been given. The mutual restrictions of water entry angle, velocity, and angle of attack on ricochet were also discussed. We find that with the increase of the angle of attack, the range of the water entry angle and the velocity used to maintain the vehicle ricochet decrease gradually.

We innovatively explore the effects of the progressive change of AUV's hemispheric angle on the water entry trajectory and find the following regular conclusions. When the AUV impacts the water at a fixed velocity, for example, $v = 100$ m/s, the smaller the angle of water entry, the more obvious the pitching motion of the vehicle's head, which indicates that the trajectory stability is worse. On the other hand, when the AUV enters the water at a fixed angle, a similar law can be found. That is, the smaller the velocity of water entry is, the more likely it is to ricochet, which also indicates that the stability of trajectory is worse. Based on our numerical simulation results, we can draw the conclusion that the trajectory characteristics of the vehicle entering the water at small angles and velocity are more sensitive to changes in the hemispheric angle of the vehicle's head. A vehicle with a hemispheric angle of approximately 70° has better trajectory stability. The results are related to the balance of pitching torque between the head and tail of the vehicle when fluid-structure interaction occurs in the process of water entry.

In addition, we also studied the influence of the angle and velocity of water entry on the trajectory of the vehicle. We find that under certain water entry initial conditions, when the water entry angle and the velocity increase, the external force direction of the model head gradually approaches the center of gravity of the model. That is to say, the model trajectory of water entry becomes more and more stable.

Data Availability

All data included in this study are available from the corresponding author upon request.

Conflicts of Interest

The authors declare that there are no conflicts of interest regarding the publication of this paper.

Acknowledgments

This study was financed by the National Natural Science Foundation of China (grant nos. 51709229 and 51879220), Natural Science Basic Research Plan in Shaanxi Province of China (grant no. 2018JQ5092), and Fundamental Research Funds for the Central Universities (grant no. 3102019JC006), and we are grateful for that.

References

[1] J. W. Nicholson and A. J. Healey, "The present state of autonomous underwater vehicle (auv) applications and technologies," *Marine Technology Society Journal*, vol. 42, no. 1, pp. 44–51, 2008.

[2] J. W. Glasheen and T. A. Mcmahon, "Vertical water entry of disks at low froude numbers," *Physics of Fluids*, vol. 8, no. 8, pp. 2078–2083, 1996.

[3] G.-X. Yan, G. Pan, Y. Shi, L.-M. Chao, and D. Zhang, "Experimental and numerical investigation of water impact on air-launched auvs," *Ocean Engineering*, vol. 167, pp. 156–168, 2018.

[4] A. May, "Water entry and the cavity-running behavior of missiles," Technical Report, Navsea Hydroballistics Advisory Committee Silver Spring Md, Baltimore, MD, USA, 1975.

[5] C. M. Seddon and M. Moatamedi, "Review of water entry with applications to aerospace structures," *International Journal of Impact Engineering*, vol. 32, no. 7, pp. 1045–1067, 2006.

[6] V. Murali and S. D. Naik, "Parametric analysis for water ricochet studies of ogive nose-shaped projectile," *The Journal of Defense Modeling and Simulation: Applications, Methodology, Technology*, vol. 11, no. 3, pp. 309–314, 2014.

[7] E. G. Richardson, "The impact of a solid on a liquid surface," *Proceedings of the Physical Society*, vol. 61, no. 4, pp. 352–367, 1948.

[8] W. Johnson and S. R. Reid, "Ricochet of spheres off water," *Journal of Mechanical Engineering Science*, vol. 17, no. 2, pp. 71–81, 1975.

[9] T. Miloh and Y. Shukron, "Ricochet off water of spherical projectiles," *Journal of Ship Research*, vol. 35, no. 2, pp. 91–100, 1991.

[10] T. T. Truscott and A. H. Techet, "Water entry of spinning spheres," *Journal of Fluid Mechanics*, vol. 625, pp. 135–165, 2009.

[11] L. Bocquet, "The physics of stone skipping," *American Journal of Physics*, vol. 71, no. 2, pp. 150–155, 2003.

[12] C. Clanet, F. Hersen, and L. Bocquet, "Secrets of successful stone-skipping," *Nature*, vol. 427, no. 6969, p. 29, 2004.

[13] L. Rosellini, F. Hersen, C. Clanet, and L. Bocquet, "Skipping stones," *Journal of Fluid Mechanics*, vol. 543, no. -1, pp. 137–146, 2005.

[14] T. T. Truscott, M. M. Wright, K. R. Langley, and J. Belden, "Holy balls! Balls that walk on water," *Physics of Fluids*, vol. 24, no. 9, Article ID 091103, 2012.

[15] J. Belden, M. A. Jandron, and T. T. Truscott, *Physics of Elastic Spheres Skipping on Water, on the Physics of Sports*, Elsevier, Amsterdam, Netherlands, 2013.

[16] M.-S. Park, Y.-R. Jung, and W.-G. Park, "Numerical study of impact force and ricochet behavior of high speed water-entry bodies," *Computers & Fluids*, vol. 32, no. 7, pp. 939–951, 2003.

[17] Y.-H. Wang and X.-H. Shi, "Numerical analysis for initial hydroballistics of airborne missile during oblique water-entry impact," *Journal of Ballistics*, vol. 24, no. 2, pp. 92–95, 2012.

[18] D. J. Benson, "Computational methods in Lagrangian and Eulerian hydrocodes," *Computer Methods in Applied Mechanics and Engineering*, vol. 99, no. 2-3, pp. 235–394, 1992.

[19] K.-J. Paik, P. M. Carrica, D. Lee, and K. Maki, "Strongly coupled fluid–structure interaction method for structural loads on surface ships," *Ocean Engineering*, vol. 36, no. 17-18, pp. 1346–1357, 2009.

[20] K. J. Maki, D. Lee, A. W. Troesch, and N. Vlahopoulos, "Hydroelastic impact of a wedge-shaped body," *Ocean Engineering*, vol. 38, no. 4, pp. 621–629, 2011.

[21] H. Xie, H. Ren, S. Qu, and H. Tang, "Numerical and experimental study on hydroelasticity in water-entry problem of a composite ship-hull structure," *Composite Structures*, vol. 201, pp. 942–957, 2018.

[22] Z. Guo, W. Zhang, X. Xiao, G. Wei, and P. Ren, "An investigation into horizontal water entry behaviors of projectiles with different nose shapes," *International Journal of Impact Engineering*, vol. 49, pp. 43–60, 2012.

[23] C. Zhao, C. Wang, Y. Wei, X. Zhang, and T. Sun, "Experimental study on oblique water entry of projectiles," *Modern Physics Letters B*, vol. 30, no. 28, Article ID 1650348, 2016.

[24] G.-X. Yan, G. Pan, Y. Shi, and G.-H. Wang, "Experimental study on water entry of cylindrical projectiles with different nose shapes," *Modern Physics Letters B*, vol. 33, no. 9, Article ID 1950107, 2019.

[25] C. Chen, X. Yuan, X. Liu, and J. Dang, "Experimental and numerical study on the oblique water-entry impact of a cavitating vehicle with a disk cavitator," *International Journal of Naval Architecture and Ocean Engineering*, vol. 11, no. 1, pp. 482–494, 2019.

[26] G.-R. Liu and M. B. Liu, *Smoothed Particle Hydrodynamics: A Meshfree Particle Method*, World Scientific, Singapore, 2003.

[27] L. B. Lucy, "A numerical approach to the testing of the fission hypothesis," *The Astronomical Journal*, vol. 82, pp. 1013–1024, 1977.

[28] R. A. Gingold and J. J. Monaghan, "Smoothed particle hydrodynamics: theory and application to non-spherical stars," *Monthly Notices of the Royal Astronomical Society*, vol. 181, no. 3, pp. 375–389, 1977.

[29] P. Maruzewski, D. L. Touzé, G. Oger, and F. Avellan, "SPH high-performance computing simulations of rigid solids impacting the free-surface of water," *Journal of Hydraulic Research*, vol. 48, no. 1, pp. 126–134, 2010.

[30] M. Anghileri, L.-M. L. Castelletti, E. Francesconi, A. Milanese, and M. Pittofrati, "Rigid body water impact-experimental tests and numerical simulations using the SPH method," *International Journal of Impact Engineering*, vol. 38, no. 4, pp. 141–151, 2011.

[31] R. Panciroli, S. Abrate, G. Minak, and A. Zucchelli, "Hydroelasticity in water-entry problems: comparison between experimental and SPH results," *Composite Structures*, vol. 94, no. 2, pp. 532–539, 2012.

[32] P. Omidvar, O. Farghadani, and P. Nikeghbali, "SPH for impact force and ricochet behavior of water-entry bodies," *International Journal of Modern Physics C*, vol. 28, no. 10, Article ID 1750119, 2017.

[33] J. J. Monaghan, "On the problem of penetration in particle methods," *Journal of Computational Physics*, vol. 82, no. 1, pp. 1–15, 1989.

[34] J. G. Waugh and G. Stubstad, *Hydroballistics Modeling*, Technical Report, Naval Undersea Center, San Diego, CA, USA, 1975.

[35] S.-L. Chuang, "Experiments on slamming of wedge-shaped bodies," *Journal of Ship Research*, vol. 11, no. 3, pp. 190–198, 1967.